

Formation of Population III stars in Fossil HII Regions: Significance of HD

Takanori Nagakura^{1,2*} and Kazuyuki Omukai¹

¹National Astronomical Observatory of Japan, Osawa, Mitaka, Tokyo 181-8588

²Department of Astronomy, The University of Tokyo, Hongo 7-3-1, Bunkyo-ku, Tokyo 113-0033

24 July 2018

ABSTRACT

We study the evolution of gas in HII regions around the first stars after the exciting stars end their lives. If the first star in a small halo dies without supernova (SN), subsequent star formation is possible in the same halo. We thus investigate the effect of ionization on subsequent star formation within small halos in the early universe using one-dimensional hydrodynamics with spherical symmetry along with non-equilibrium primordial gas chemistry. We find that the enhanced electron fraction facilitates the formation of molecular hydrogen at the cores of these halos. The low temperature circumstances produced by the H_2 cooling is favorable to HD formation and the resultant cooling further drops the temperature below 100 K. Consequently, low-mass stars with primordial abundances can form even in a small halo. After accreting the interstellar metals, these stars might resemble low-mass ultra metal-poor stars discovered in the present-day Galactic halo.

Key words: cosmology:theory – galaxies:formation – HII regions – molecular processes – stars:formation

1 INTRODUCTION

Observations of high- z quasars indicate that the intergalactic medium (IGM) was ionized at $z > 6$. In addition, the recent *Wilkinson Microwave Anisotropy Probe* (WMAP) observations suggest that the universe was reionized as early as $z \sim 17$ (Kogut et al. 2003). It is still unclear what astrophysical phenomena caused the reionization of the universe, but photoionization by massive stars is among the most promising candidates. It is hence important to study the star formation in the early universe. The first generation of stars was formed out of unmagnetized gas of primordial composition, which leads to simplification of the relevant physics. On the other hand, the formation processes of second-generation stars are more complex because of various feedback effects from the first stars, for example, radiative heating and ionization/dissociation, metal enrichment, secondary density and velocity fluctuations etc. (e.g., Ciardi & Ferrara 2004). For reliably predicting the star formation history and the initial mass function (IMF), etc., it is crucial to understand various feedback effects in the high-redshift universe.

In the context of cold dark matter (CDM) cosmology, the first collapsed objects are predicted to have masses corresponding to virial temperature $T_{\text{vir}} < 10^4 \text{K}$ (hereafter, we refer to such objects as “small halos”). In such halos, gas cools and contracts further to form stars only via H_2 rovibrational emission. The first stars, which formed in small halos, are indicated to have masses of a few hundreds M_\odot (Abel, Bryan & Norman 2002; Bromm, Coppi & Larson

2002; Omukai & Palla 2003). Once such a massive first star forms in a small halo, an enormous amount of ionizing photons from the star ionizes its surrounding gas (Whalen, Abel & Norman 2004; Kitayama et al. 2004) and photodissociates the molecular hydrogen. Consequently, star formation in the same halo is completely suppressed (Omukai & Nishi 1999; Glover & Brand 2001). After that, depending on the mass, the central star will explode as a SN or collapse directly into a BH at the end of its lifetime. Zero-metal stars in the ranges $10 - 40 M_\odot$ and $140 - 260 M_\odot$ explode as type II SNe or pair-instability SNe, respectively (Heger & Woosley 2002; Umeda & Nomoto 2002). The ashes of these first SNe pollute their surrounding gas with metals and dust grains, out of which subsequent generations of low-mass stars form (Bromm et al. 2001; Schneider et al. 2002; Omukai et al. 2005). However, more often than not, the first stars directly form BHs without SNe since the stellar mass range that causes SNe is rather limited. After the death of the exciting star, ionized gas in the HII region begins to recombine. We call such an ex-HII region after the death of the exciting star a fossil HII region (after Oh & Haiman 2003). In shock ionized gas in large halos at virialization and SN shells, formation of H_2 and HD molecules are promoted (Mac Low & Shull 1986; Shapiro & Kang 1987; Yamada & Nishi 1998). A similar situation can happen also in a fossil HII region. High ionization degree there facilitates formation of H_2 via the H^- channel. The gas can cool and contract owing to the H_2 cooling, thereby producing a subsequent generation of stars in the same halo. In particular, in those halos, more H_2 is formed and then lower temperature is achieved than in the first star formation because of the initial ionization. The enhanced

* E-mail: nagakura@th.nao.ac.jp (TN) ; omukai@th.nao.ac.jp (KO)

H₂ cooling and resultant lower temperature environment facilitates HD formation. Although the mass of primordial stars is often supposed to be very high, HD cooling, if it becomes important, enables the formation of low-mass stars (Uehara & Inutsuka 2000; Nakamura & Umemura 2002).

The problems we try to solve in this paper are the following: Does the ionized primordial gas in a small halo cool and subsequently form stars again inside the same halo? Does HD work as an efficient coolant in such situations? To tackle these problems, we treat the gas as one-dimensional spherically symmetric fluid and follow the evolution with solving chemical reactions in primordial gas.

This paper is organized as follows: Section 2 describes the numerical model used in this paper. Section 3 presents the results of our simulation, and Section 4 is devoted to the discussion. Finally, we summarize our conclusions. Throughout this paper, we adopt a flat Λ CDM cosmology with density parameters $\Omega_\Lambda = 0.73$, $\Omega_m = 0.27$, $\Omega_b = 0.044$ and the Hubble parameter $h = 0.71$ (Spergel et al. 2003).

2 THE MODEL

As an evolution of fossil HII regions, which were once stellar ionized regions but now are recombining because of the death of the exciting stars, within small halos in the early universe, we envisage the following scenario. First, the first star forms at the center of a small halo. Then, an enormous amount of ionizing flux from the first star forms an HII region. During the lifetime of the exciting star, the radius of gas accelerated by high pressure of the ionized gas reaches $\sim c_s t_{\text{OB}} \sim 50(T/2 \times 10^4 \text{K})^{1/2} (t_{\text{OB}}/3 \text{Myr}) \text{pc}$, where c_s , t_{OB} are the sound speed of the gas and the lifetime of a massive star, respectively, while the HII region itself extends to an even larger radius. Note that despite the shallow potential well of a small halo, photoevaporation does not always occur: since the HII region is smaller than the radius of the halos, gas can avoid photoevaporation if cooling takes place immediately. If the star explodes as a SN at the end of its lifetime, the gas inside these halos will be swept out by its blast wave (Bromm, Yoshida & Hernquist 2003; Wada & Venkatesan 2003). However, here we consider the case where the central star directly forms a BH without a SN explosion. Specifically, we calculate the evolution of the ionized gas starting from the state after the death of the central star (Whalen et al. 2004; Kitayama et al. 2004). We employ one-dimensional hydrodynamics with spherical symmetry along with primordial gas chemistry. In this simulation, we ignore any influence of a relic BH, which resides in the central region of the halo, on its surrounding gas, for simplicity. In reality, accretion onto the BH generates some photodissociative radiation. According to O’Shea et al. (2005), however, this does not affect the H₂ formation in the halo significantly. The gravitational effect of the BH is assessed from its Bondi accretion radius in this paper. At the outer boundary, since our interest is the central region of the gas, we take the gas radius to be 200 pc, which is the radius of the expanding region according to Whalen et al. (2004)’s results, and set the pressure outside the cloud to be zero. This setting means that only the accelerated region inside the HII region is considered: the matter outside is neglected whether it is ionized or not. We have also performed runs with a gas radius of 1 kpc that corresponds to the whole HII region and have confirmed that our results remain almost unaltered for the halo mass $\gtrsim 10^6 M_\odot$.

2.1 Hydrodynamics

We assume spherical symmetry, and neglect both magnetic field and external radiation field except for cosmic microwave background (CMB) radiation. The basic equations of one-dimensional spherically symmetric fluid are the following:

$$\frac{dM_b}{dr_b} = 4\pi r_b^2 \rho_b, \quad (1)$$

$$\frac{d^2 r_b}{dt^2} = -4\pi r_b^2 \frac{dp}{dM_b} - \frac{GM(r_b)}{r_b^2} + \Omega_\Lambda H_0^2 r_b, \quad (2)$$

$$\frac{du}{dt} = \frac{p}{\rho_b^2} \frac{d\rho_b}{dt} - \frac{\Lambda}{\rho_b}, \quad (3)$$

$$p = (\gamma - 1)\rho_b u = \frac{k_B \rho_b T}{\mu m_p}, \quad (4)$$

where r_b , M_b , ρ_b , p , T , u , μ , $M(r_b)$, G , k_B , Ω_Λ , H_0 , Λ are the radius, mass, density, pressure, temperature, internal energy per unit mass, mean molecular weight in units of the proton mass m_p , the total mass interior to r_b , the gravitational constant, the Boltzmann constant, the cosmological constant, the Hubble parameter at the present-day, and the cooling rate per unit volume, respectively. The last term of the right-hand side in the second equation represents the correction of the expanding universe. The adiabatic index γ , which depends on chemical abundances, is calculated at each time-step. We here neglect the chemical heating/cooling term because it is not important in the density range we considered ($< 10^8 \text{cm}^{-3}$).

We solve these equations using the standard second-order-accurate Lagrangian finite-difference scheme with von Neumann-Richtmyer artificial viscosity (e.g., Mihalas & Mihalas 1984; Thoul & Weinberg 1995; Omukai & Nishi 1998). The grids are spaced unequally in mass. The innermost cell contains $3.7 \times 10^{-6} M_\odot$, and the increments in radius between adjacent grid cells are increased by 5% outwardly. We take 100 cells and have confirmed that it is enough to follow the evolution near the center.

2.2 Dark Matter

We need to determine the dark-matter distribution to solve a set of hydrodynamic equations. We assume that the dark-matter distribution is fixed in time since dark matter has already virialized at the phase that we are interested in. We adopt the dark-matter density profile derived by Navarro, Frenk & White (1997):

$$\rho(r) = \frac{\rho_{\text{crit}} \delta_c}{r/r_s (1 + r/r_s)^2}, \quad (5)$$

where ρ_{crit} , δ_c , r_s are the critical density at virialization redshift, characteristic dimensionless density at the center and characteristic radius, respectively. This density profile has the following three parameters: the mass of a dark matter halo M_{halo} , the virialization redshift z_{vir} of the halo, and the concentration parameter c , which expresses the concentration of mass near the center of the halo. In particular, by using c , the virial radius of the halo $r_{\text{vir}} = cr_s$. Here we fix $c = 5$ because its small variation does not affect our results.

2.3 Cooling Processes

We incorporate rovibrational line cooling of H₂ and HD, Ly α line cooling of atomic hydrogen, and Compton cooling by CMB radiation since we consider the temperature range $< 2 \times 10^4$ K. For line cooling of H₂ we adopt the fitting function given by Galli & Palla (1998). HD cooling rate is calculated by solving the statistical equilibrium between the first 5 rotational levels. The radiative and

collisional transition rate coefficients are the same as those in Galli and Palla (1998). Ly α line cooling rate of atomic hydrogen is given by (Dalgarno & McCray 1972)

$$\Lambda_{\text{Ly}\alpha} = 7.5 \times 10^{-19} \exp\left(-\frac{1.18 \times 10^5 \text{K}}{T}\right) n(e)n(H) \quad \text{erg s}^{-1} \text{cm}^{-3}, \quad (6)$$

where $n(H)$ is the number density of neutral hydrogen. The Compton cooling rate is given by (e.g., Rybicki & Lightman 1979)

$$\Lambda_{\text{Compton}} = \frac{4k_{\text{BC}}\sigma_T n(e)U_\gamma(T - T_\gamma)}{m_e c^2} = 1.017 \times 10^{-37} T_\gamma^4 (T - T_\gamma) n(e) \quad \text{erg s}^{-1} \text{cm}^{-3}, \quad (7)$$

where c , σ_T , $n(e)$, U_γ , T_γ are the speed of light, Thomson scattering cross section, number density of electron, energy density of photon and photon temperature, respectively. When the gas temperature decreases as low as the CMB temperature T_γ , the heating by the radiation becomes important. We include this effect by replacing the radiative cooling rate Λ with $\Lambda(T) - \Lambda(T_\gamma)$.

2.4 Chemical Reactions

We need to solve chemical reactions as well as hydrodynamic equations since cooling of the gas depends on chemical abundances of the coolants. We assume that the reactions are only two-body collisional ones and do not include the three-body H₂ formation process because we consider only the low density range ($n_H < 10^8 \text{cm}^{-3}$). The evolution of chemical species i is followed by solving the kinetic equation

$$\frac{dn(i)}{dt} = -n(i) \sum_j k_{ij} n(j) + \sum_{l,m} k_{lm} n(l)n(m), \quad (8)$$

where k_{ij} and k_{lm} are the reaction rate coefficients of destruction and those of formation, respectively.

Since no pollution of the gas with metals has taken place in this situation, we consider the following 14 species: H, H⁺, H⁻, H₂, H₂⁺, He, He⁺, He⁺⁺, e⁻, D, D⁺, D⁻, HD, HD⁺. The fractions of He and D atoms are assumed to be 0.0833 and 2.5×10^{-5} , respectively, which are inferred from big bang nucleosynthesis (Romano et al. 2003). Reactions among H and He compounds and their rate coefficients are the same as those in Abel et al. (1997). For D reactions, we adopt the compilation by Nakamura & Umemura (2002), although we replace the rate coefficients of the reactions D5, D9, D10 and D11 with those by Galli & Palla (2002). The total number of considered reactions amounts to 37. We solve the rate equations for 14 species above using an implicit difference scheme.

2.5 Initial and Boundary Conditions

We assume that the first star in a small halo is formed around the time of virialization. The initial epoch of our calculation is after 3 Myr, the typical lifetime of massive stars, of virialization. The evolution of the first HII regions in the early universe has been studied by Whalen et al. (2004) and Kitayama et al. (2004). We construct the initial density and velocity distributions following Whalen et al. (2004)'s results. Their results show that, inside the HII region, there are two distinct regions: the inner region is expanding with outwardly increasing velocity and the velocity reaches the sound speed of the ionized gas at a radius of ~ 200 pc, while the gas outside is almost unaccelerated. We consider only the expanding

region in our calculation. Also, according to Whalen et al. (2004), the density distribution inside that region is almost constant ($\sim 0.06 \text{cm}^{-3}$), and the velocity increases gradually from the center outward. As the fiducial runs, we assume that the density profile of gas is constant at 0.06cm^{-3} , and that the velocity is proportional to the radius. At 200 pc from the center, the velocity is about sound speed. There is no gas outside this region. We set the initial gas temperature inside the HII region to be 2×10^4 K. The gas is assumed to be fully ionized initially.

This initial condition corresponds to the total baryonic mass of $6 \times 10^4 M_\odot$ in the fiducial cases. In the case of $10^5 M_\odot$ halos, this condition leads to too much baryon compared to dark matter. Probably a lower gas-density state is more appropriate as an initial condition for such a small halo. Our choice of the initial condition facilitates the cloud to cool and contract. Even with this favorable condition, however, they do not cool anyway as described later. Then, the results do not change even if the initial gas density is lowered. For simplicity, we use the same initial condition for baryons in all the cases.

The size of the flat density region (~ 200 pc) is basically the sound speed in the HII region c_s times the lifetime of the exciting stars t_{OB} . Although the size of the flat density region does not depend significantly on halo quantities, there should still be some density variations among halos. To study the effect of different initial gas densities, we also calculate the cases where the initial gas density is either halved or doubled from the fiducial value.

We follow the evolution until the local Hubble time at z_{vir} passes or the central number density reaches the threshold value 10^8cm^{-3} . When the latter condition is satisfied, we regard the gas to have cooled and collapsed. We take the threshold density at 10^8cm^{-3} , since three-body H₂ formation, which we do not include here, becomes important for higher densities and the evolution cannot be followed correctly thereafter. The results do not depend on the value of the threshold density as long as the free-fall time there is sufficiently shorter than the local Hubble time.

3 RESULTS

We simulate the evolution of ionized primordial gas in small halos of different masses and formation redshifts. The parameters of the runs that we have performed are listed in Table 1.

We first show the case where the dark halo virializes at $z_{\text{vir}} = 15$ and its mass $M_{\text{halo}} = 10^7 M_\odot$. Hereafter we call this case our fiducial model. In Figure 1, we show the evolution of the number density, temperature, mass, and velocity distributions. The numbers from 0 to 5 in this figure represent the time sequence. State 0 corresponds to the initial distribution. The numbers are assigned every time when the central density reaches 100 times that of the previous numbered state. The numbers from 1 to 5 correspond to the states after 7.94 Myr, 2.90 Myr, 1.93 Myr, 713 kyr and 47.7 kyr of the previous state, respectively. The time passed from 0 to 5 is 13.5 Myr and $z \approx 14.4$ at state 5. The central evolution is shown in Figure 2. In this figure, we plot the evolution of chemical abundances and cooling/heating rates as functions of the central number density. In Figure 3, we plot the central temperature against the central number density along with cases of different halo sizes. In the fiducial case, the number density at the center reaches 10^8cm^{-3} within the local Hubble time at $z = 15$ ($\sim 4.1 \times 10^8$ yr), namely, the cloud has cooled and collapsed successfully.

Without dark matter, the density distribution of collapsing clouds is known to follow the Larson-Penston-type similarity so-

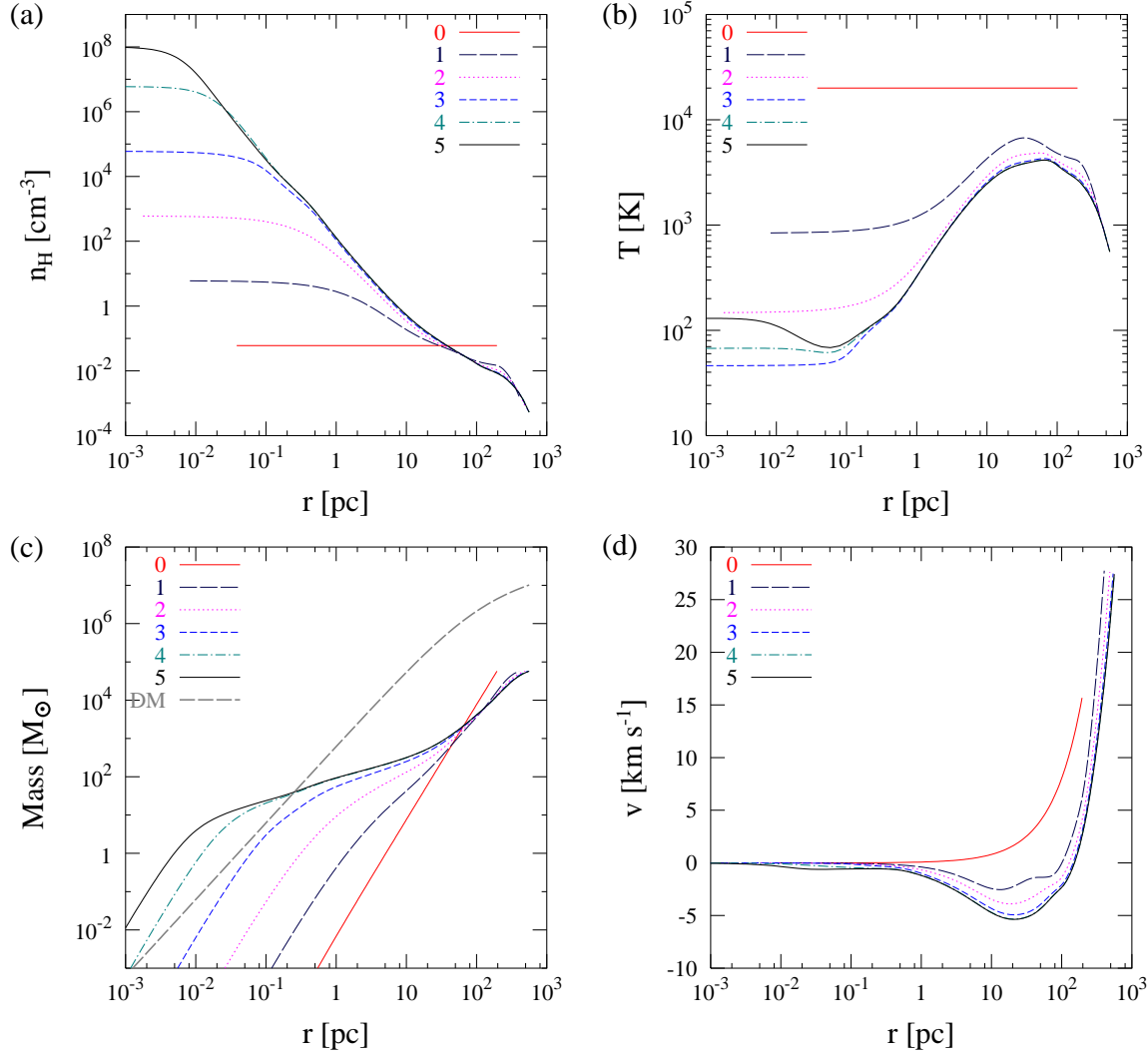
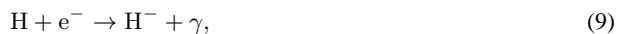


Figure 1. The evolution of the number density (a), temperature (b), mass (c), velocity distribution (d) as a function of the radius for the fiducial run ($z_{\text{vir}}=15$, $M_{\text{halo}}=10^7 M_{\odot}$). The numbers represent the evolutionary sequence, and we set our initial state as state 0. The numbers from 1 to 5 correspond to the states after 7.94 Myr, 2.90 Myr, 1.93 Myr, 713 kyr, 47.7 kyr from the previous ones. Each state we numbered has central density 100 times larger than that of the previous state. In panel (c), we also plot the dark-matter mass distribution (indicated as “DM”). The initial low gas density ($\sim 0.1 \text{ cm}^{-3}$) reflects our choice of the initial state, which is the gas inside the HII region. Since we consider only the matter inside the radius of 200 pc, the total gas mass in our calculated region is lower than that in the halo ($(\Omega_b/\Omega_m)M_{\text{halo}} \sim 1.7 \times 10^6 M_{\odot}$).

lution (Larson 1969; Penston 1969). This solution consists of two regions, i.e., a core with flat density distribution and an envelope with outwardly decreasing density. The diameter of the core is approximately the Jeans length $\lambda_J \sim c_s / \sqrt{\rho_{\text{gas}}}$. In our case, we need to consider the dark matter gravity. In Figure 1 (a), we see that the density distribution is similar to the Larson-Penston type solution, but the core radius is smaller. Owing to the dark matter contribution, the core radius is about $c_s / \sqrt{\rho_{\text{gas}} + \bar{\rho}_{\text{DM}}}$, where $\bar{\rho}_{\text{DM}}$ is the dark-matter density averaged in the core. This means that dark matter reduces gas density in the collapsing clouds. The small bent in the density distribution at ~ 0.1 pc corresponds to the transition from the dark matter to the self-gravity dominance.

A large amount of molecular hydrogen is immediately formed (Figure 2 a) through the H^- channel



because the electron, which is the catalyst of this reaction, is abundant in our initial state. On the other hand, the electron fraction declines dramatically through recombination with increasing density. Because of the reduced number of electrons, the abundance of molecular hydrogen becomes saturated. Around the center, the H_2 fraction finally reaches about 5×10^{-3} , which is well above that in the case of a halo without initial ionization (about 10^{-4} for $n_{\text{H}} \lesssim 10^4 \text{ cm}^{-3}$; e.g., Abel et al. 2002). In our case, the temperature drops enough to trigger HD formation. The resultant HD cooling reduces the temperature below 100 K (see Figures 1 b and 3). The total mass of the region that is eventually cooled below 100 K amounts to $\sim 28 M_{\odot}$.

Note that the gas in small halos with $T_{\text{vir}} < 10^4$ K will be photoevaporated unless it cools below T_{vir} by molecular cooling within a sound-crossing time. Our results indicate that, even in such small halos, some clouds can contract without photoevaporation owing to the instant effect of H_2 cooling.

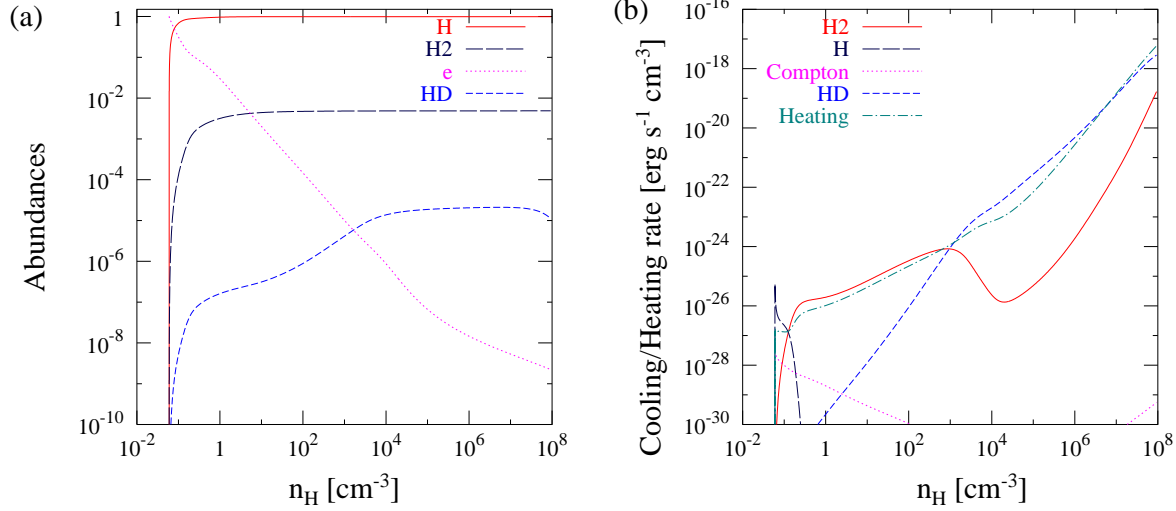


Figure 2. The evolution of the chemical species (a) and the cooling/heating rates (b) at the center for the fiducial run ($z_{\text{vir}}=15, M_{\text{halo}}=10^7 M_{\odot}$). In panel (a), the H, H₂, HD and electron fractions at the center is shown as a function of the central number density. In panel (b), the H Ly α cooling, the H₂ cooling rate, the HD cooling rate, the Compton cooling and the compressional heating rate per unit volume are plotted.

z_{vir}	$M_{\text{halo}} [M_{\odot}]$	$T_{\text{vir}} [\text{K}]$	$\Delta t [\text{yr}]$	z_{end}	cooled ?
15	10^5	1.6×10^2	–	–	No
	10^6	7.6×10^2	1.65×10^8	10.7	Yes
	10^7	3.5×10^3	1.35×10^7	14.4	Yes
	10^8	1.6×10^4	4.67×10^6	14.7	Yes
20	10^5	2.1×10^2	–	–	No
	10^6	1.0×10^3	5.25×10^7	16.6	Yes
	10^7	4.6×10^3	7.76×10^6	19.2	Yes
	10^8	2.1×10^4	3.08×10^6	19.6	Yes
25	10^5	2.7×10^2	–	–	No
	10^6	1.2×10^3	2.56×10^7	21.9	Yes
	10^7	5.7×10^3	5.44×10^6	23.9	Yes
	10^8	2.7×10^4	2.29×10^6	24.3	Yes
30	10^5	3.2×10^2	–	–	No
	10^6	1.5×10^3	1.59×10^7	26.7	Yes
	10^7	6.8×10^3	4.23×10^6	28.6	Yes
	10^8	3.2×10^4	1.82×10^6	29.1	Yes

Table 1. The list of our runs. We list the virialization redshift, the halo mass, the virial temperature, the time elapsed in our simulation, the redshift at the end of our simulation, and whether the gas can cool or not.

Figure 2 (b) shows the contribution to the cooling rate by important coolants in the course of the contraction. Also shown is the compressional heating rate. At the initial state, because the gas temperature is 2×10^4 K, the Ly α line cooling of atomic hydrogen is the most effective. Below 10^4 K the Ly α line cooling is cut off since the atomic hydrogen becomes very hard to excite. Then, H₂ cooling, which compensates compressional heating subsequently, enables further contraction of the gas. When the temperature decreases below 200 K at 10^3 cm^{-3} , molecular hydrogen is no longer excited and its cooling rate declines rapidly. The low temperature at this point is sufficient to trigger abundant HD production (see Figure 2 a).

The HD abundance is determined by equilibrium between the

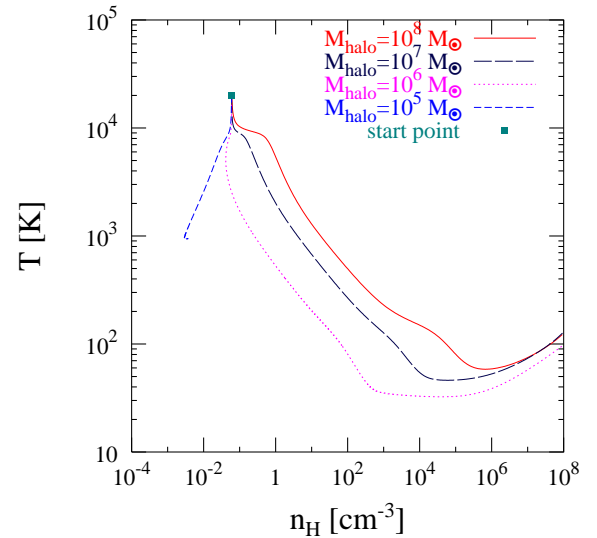
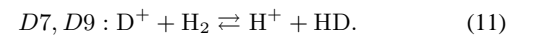


Figure 3. The evolution of the central temperature as a function of the central number density for halos with $z_{\text{vir}} = 15$. We plot the cases of $M_{\text{halo}} = 10^5, 10^6, 10^7,$ and $10^8 M_{\odot}$. The square represents the initial state.

formation rate and its reverse rate (e.g., Omukai et al. 2005),



By equating rates of these reactions,

$$\frac{n(\text{HD})}{n(\text{H}_2)} = \frac{k_{D7}n(D^+)}{k_{D9}n(H^+)}, \quad (12)$$

where k_{D7} and k_{D9} are the forward and its reverse reaction rate coefficients respectively. The abundance of D^+ is given by the equilibrium between the following reactions:



Similarly,

$$\frac{n(D^+)}{n(H^+)} = \frac{k_{D2}n(D)}{k_{D3}n(H)}. \quad (14)$$

From equations (12) and (14), the HD to H₂ ratio is given by

$$\frac{n(\text{HD})}{n(\text{H}_2)} = \frac{k_{D2}k_{D7}n(\text{D})}{k_{D3}k_{D9}n(\text{H})} = 2 \exp\left(\frac{421\text{K}}{T}\right) \frac{n(\text{D})}{n(\text{H})}. \quad (15)$$

For the numerical value, we used the rate coefficients compiled by Nakamura & Umemura (2002). The equation (15) tells that because the binding energy of HD is higher than that of H₂ by $\Delta E/k_B = 421\text{K}$, HD is a state preferable to H₂ at the low temperature. Therefore the HD formation is promoted in an environment where the temperature is much lower than the difference of binding energies.

After the temperature falls below 200 K, HD becomes the dominant coolant and its cooling exceeds the compressional heating. Then the temperature continues to decrease and eventually reaches below 100 K. This trend continues until the number density 10^5 cm^{-3} , which is the critical density for HD to reach the local thermodynamic equilibrium (LTE). The HD cooling rate per unit mass subsequently saturates and temperature begins to increase with the compressional heating now exceeding the HD cooling (see Figure 2 b).

Let us evaluate mass of the cooled region at the center of the cloud, which is expected to become stars eventually. For gas to contract and fragment into stars, it must be bounded by its self-gravity. The condition for the gas self-gravity dominating the dark matter gravity within the radius r is that the enclosed gas mass $M_{\text{gas}}(r)$ is larger than the enclosed dark matter mass $M_{\text{DM}}(r)$. We hereafter refer to a central portion satisfying the condition above as a central cooled region. For the fiducial run, we plot the gas mass and the dark matter mass as a function of the radius in Figure 2 (c). From this, we see that the radius of the central cooled region is about 0.27 pc and the gas mass contained there is about $45 M_\odot$.

In Figure 4, we show the evolution of H₂, HD and electron distributions. The region of high H₂ fraction ($\gtrsim 10^{-3}$) is as large as $10^4 M_\odot$. Within the central $\sim 100 M_\odot$, $y(\text{H}_2)$ reaches 5×10^{-3} , while the electron is significantly depleted. In the central $\sim 10 M_\odot$, D becomes fully molecular. In the outermost region, although the electron is abundant, H₂ formation is suppressed because of very low density. The temperature decrease ($< 10^4 \text{ K}$) there is caused by the expansion of the gas as well as by the Ly α line cooling and the Compton cooling.

We also calculated the cases where the initial gas density is halved and doubled. In such cases, the gas evolution is qualitatively very similar to our fiducial case. The size and mass of the central cooled regions in these cases are also similar to those of the fiducial case. Their differences from the fiducial case are within a factor of 2 in mass. In the halved density case the size and mass are $\sim 0.22 \text{ pc}$ and $\sim 31 M_\odot$, while in the doubled density case they are $\sim 0.35 \text{ pc}$ and $\sim 77 M_\odot$, respectively. We conclude that the effect of different initial density on the size and mass of the cooled region is small, although present to some extent.

Next, we discuss the run with $z_{\text{vir}} = 15$ and $M_{\text{halo}} = 10^8 M_\odot$, where the dark halo mass is ten times larger than our fiducial one. The central temperature evolution has been presented in Figure 3. Also in this case, the central number density reaches 10^8 cm^{-3} within the Hubble time at $z_{\text{vir}} = 15$: by our criterion, the cloud has cooled and collapsed. The density and temperature evolve in a fashion similar to that of the fiducial case. The time required to collapse is, however, several times smaller because of the deeper potential well: the total elapsed time is about 4.7 Myr and $z \sim 14.7$ at the final state. The temperature, chemical abundances, and cooling/heating rates also qualitatively behave as in the fiducial run, but the cooling/heating rates are larger by two orders of magni-

z_{vir}	$M_{\text{halo}} [M_\odot]$	Radius [pc]	Mass [M_\odot]
15	10^6	0.31	30
	10^7	0.27	45
	10^8	0.16	35
20	10^6	0.28	40
	10^7	0.19	39
	10^8	0.11	28
25	10^6	0.24	46
	10^7	0.14	35
	10^8	0.09	27
30	10^6	0.22	50
	10^7	0.12	34
	10^8	0.07	27

Table 2. The radius and mass of the central cooled region in our runs. From the left, we list the virialization redshift, the halo mass, the radius and the gas mass of the central cooled region.

tude. This is because the shorter collapse time and the consequent higher compressional heating keep the temperature higher than in the fiducial run (see Figure 3). By $n_{\text{H}} \gtrsim 10^6 \text{ cm}^{-3}$ the evolution of temperature and then cooling rate has converged with that in the fiducial run. The evolution in the cases of smaller halo masses with the same virialization redshift is as follows: For a halo with $10^6 M_\odot$, the gas cools and collapses within the local Hubble time, while that in a halo with $10^5 M_\odot$ does not. For the halo of $10^5 M_\odot$ and initially also for that of $10^6 M_\odot$, the number density decreases because of the initial expanding motion. For the halo with $10^6 M_\odot$, the initially expanding gas eventually cools and contracts enough within the Hubble time while for the halo with $10^5 M_\odot$ the gas continues expanding owing to shallow potential well.

So far, we have seen the results for halos virializing at $z = 15$. The case for the halo virializing earlier ($z = 30$) with smaller mass ($10^6 M_\odot$) closely resembles our fiducial run. This is because the earlier a halo virializes, the more dark matter tends to concentrate at the center of a halo. Consequently, increasing z_{vir} cancels decreasing M_{halo} . We perform additional runs with $z_{\text{vir}} = 20$ and 25 for $M_{\text{halo}} = 10^5, 10^6, 10^7$ and $10^8 M_\odot$ in order to see whether or not the ionized gas within these halos cools and collapses. We summarize the results for all runs in Figure 5 and in Table 1. Roughly speaking, the gas in a fossil HII region collapses and forms stars again if the halo mass is larger than $10^6 M_\odot$. We also summarize the size and the gas mass of the central cooled regions for all runs in Table 2. The size of the central cooled region becomes smaller with increasing the halo mass because the collapse time-scale becomes shorter (Table 1) and there is not enough time to cool.

Here we have included only the initially expanding gas in our simulation boundary. In reality, a large amount of the static material exists just outside the boundary. If we include it, the expanding gas will collide with it and will be decelerated. Then, the collapse of the gas is facilitated. Consequently, even the gas in halos smaller than $10^6 M_\odot$, which could not cool in our runs, might be able to collapse and form stars in more realistic calculations.

4 DISCUSSIONS

We have shown that the temperature in a fossil HII region of the first star drops as low as the CMB temperature by HD cooling even

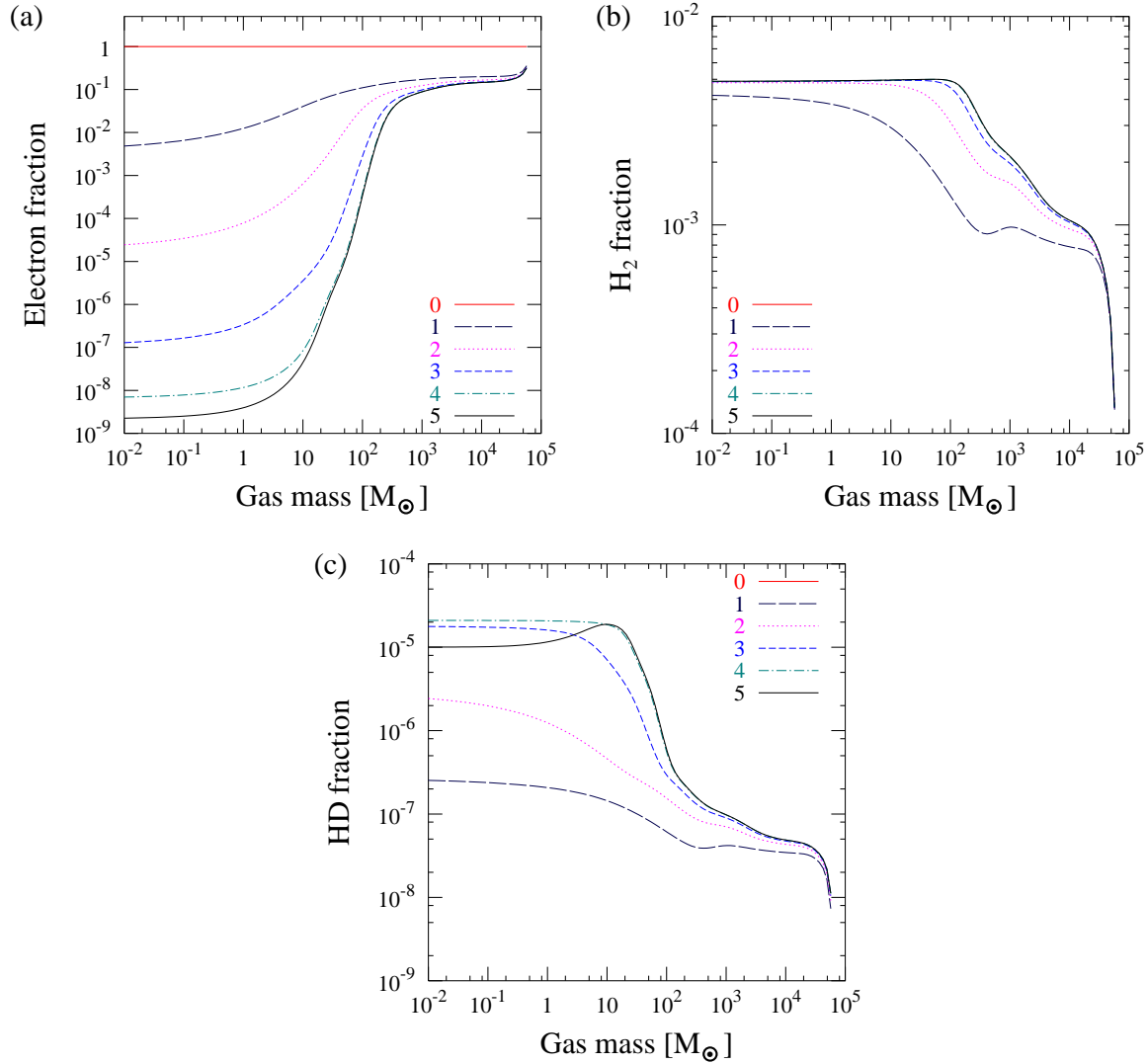


Figure 4. The evolution of the electron, H_2 , and HD fraction as a function of the Lagrangian gas-mass coordinate for the fiducial run ($z_{\text{vir}}=15$ and $M_{\text{halo}}=10^7 M_{\odot}$). The numbers have the same meaning as those in Figure 1.

with the primordial composition. In the case of the formation of first-generation stars, HD does not become important and such a low temperature is not attained (Bromm et al. 2002). In our situation, the high electron fraction enables molecular hydrogen to form in a larger amount than in an initially un-ionized cloud. Abundant H_2 molecules thus formed cool the gas below the threshold temperature for HD formation ($\sim 150\text{K}$; Omukai et al. 2005). Under such a low temperature environment, with further contraction the gas is expected to fragment into low-mass ($\sim 0.1 - 2 M_{\odot}$) gas clumps (Uehara & Inutsuka 2000; Nakamura & Umemura 2002). Uehara & Inutsuka (2000) claimed that subsolar mass stars are formed by HD cooling in a cooled layer behind an ionizing shock due to either virialization or a SN. In the case of a virialization shock, the halo must be massive enough to cause a strong shock. When such large halos are formed in the standard bottom-up scenario of structure formation, star formation and metal-enrichment may have proceeded in building blocks. Similarly, in the case of SN shocked layers, metal-pollution might have taken place at the explosion. Therefore, it is not certain whether the gas in such shock-ionized region remains metal-free. On the other hand, here we have proposed a viable sce-

nario for forming low-mass stars from primordial pristine gas. If those low-mass stars accrete metal-polluted interstellar medium after the formation, they might resemble ultra metal-deficient stars (e.g., Yoshii 1981). This may explain the origin of the ultra metal-deficient low-mass stars discovered recently (Christlieb et al. 2002; Frebel et al. 2005).

Here, we estimate the number of second-generation stars forming in a fossil HII region. The mass of the central cooled clump M_{clump} is about $45 M_{\odot}$ in the fiducial run (Section 3). By using the star formation efficiency ϵ_* and the typical mass-scale of the second-generation stars M_* , the number of the second-generation stars is

$$N_* = \epsilon_* M_{\text{clump}} / M_* = 5 \left(\frac{\epsilon_*}{0.1} \right) \left(\frac{M_{\text{clump}}}{50 M_{\odot}} \right) \left(\frac{M_*}{1 M_{\odot}} \right)^{-1}. \quad (16)$$

A few second-generation stars are formed per each first star if they are in relatively massive ($\gtrsim 10^6 M_{\odot}$) halos.

Next, we evaluate the accretion rate onto the protostars. As mentioned in Section 3, the core radius becomes $r_{\text{core}} \sim$

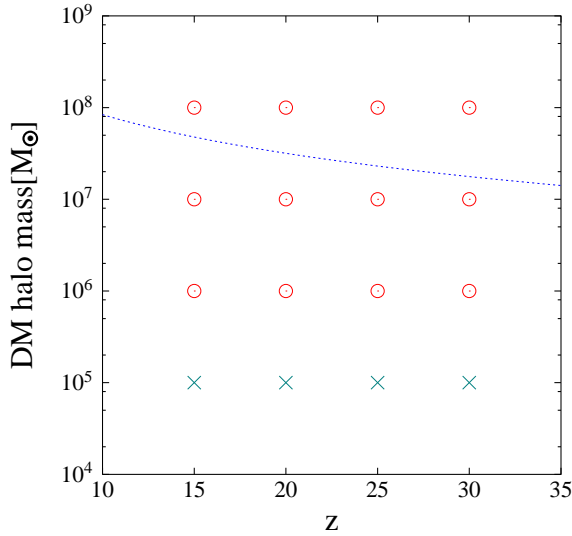


Figure 5. The $z_{\text{vir}} - M_{\text{halo}}$ diagram showing whether the ionized gas in the halos of virialization redshift z_{vir} and mass M_{halo} can cool and collapse or not. The cases where the gas cools and collapses within the local Hubble time are shown by the circles, while the other cases are by the crosses. The dotted line represents $T_{\text{vir}} = 10^4$ K, objects below which are “small halos”.

$c_s / \sqrt{\rho_{\text{gas}} + \bar{\rho}_{\text{DM}}}$ in the presence of dark matter. Assuming the gas mass in the core $M_{\text{gas}} \sim \rho_{\text{gas}} r_{\text{core}}^3$ falls into the center in the free-fall time $t_{\text{ff}} \sim 1 / \sqrt{G(\rho_{\text{gas}} + \bar{\rho}_{\text{DM}})}$, the accretion rate becomes

$$\dot{M} \sim \frac{M_{\text{gas}}}{t_{\text{ff}}} \sim \frac{\rho_{\text{gas}} r_{\text{core}}^3}{\{G(\rho_{\text{gas}} + \bar{\rho}_{\text{DM}})\}^{-1/2}} \sim \left(\frac{\rho_{\text{gas}}}{\rho_{\text{gas}} + \bar{\rho}_{\text{DM}}} \right) \frac{c_s^3}{G}. \quad (17)$$

Namely, when dark matter dominates the gravity, the accretion rate becomes smaller than that without dark matter by a factor of $\rho_{\text{gas}} / (\rho_{\text{gas}} + \bar{\rho}_{\text{DM}})$. In Figure 6, we show the mass accretion rate by equation (17) for the fiducial run. As a time coordinate, we use the mass of the central star, i.e., the gas mass that has already accreted at a given time. Also shown for comparison is c_s^3 / G , which is the accretion rate without dark matter (Shu 1977). Initially, the effects of dark matter is weak in the accretion rate because the self-gravity dominates in the inner part. The accretion rate is about $10^{-4} M_{\odot} / \text{yr}$. This is smaller than that in the first star formation, $\sim 10^{-3} - 10^{-2} M_{\odot} / \text{yr}$ because of the lower temperature resulting from HD cooling. Later the discrepancy from c_s^3 / G becomes significant because of dominant dark-matter gravity: the accretion rate by equation (17) remains $\sim 10^{-4} M_{\odot} / \text{yr}$, while c_s^3 / G becomes large owing to the higher temperature in the outer part. Note that such an outer portion is outside the central cooled region since the dark-matter gravity is dominant.

Recently, O’Shea et al. (2005) studied the evolution of a fossil HII region from a similar initial condition to ours. Their conclusion agrees with ours in the respect that the enhanced electron fraction promotes H_2 formation and the resultant lower temperature enables formation of lower mass stars than the first-generation stars. Since they utilized detailed three-dimensional hydrodynamics, their calculation is superior to ours with respect to the dynamics. However, they did not include deuterium chemistry, which is found to be important in our calculation. In this regard, our calculation is complementary to theirs. They discussed the mass scale of the second-generation stars by comparing the accretion timescale $t_{\text{acc}} = M_* / \dot{M}$ with the Kelvin-Helmholtz timescale

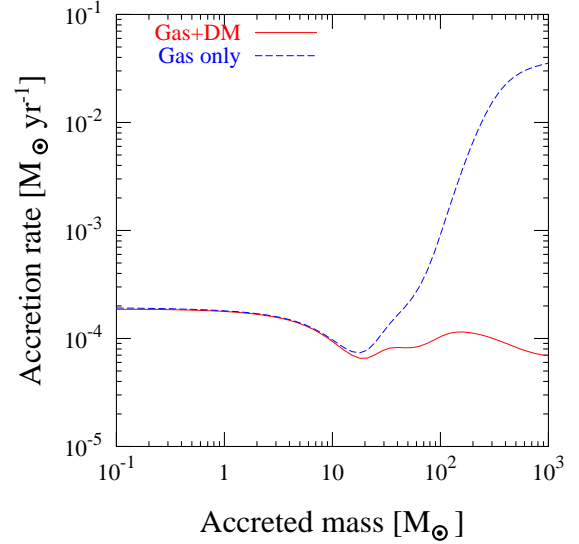


Figure 6. Evolution of the mass accretion rate onto the protostar forming in the fossil HII region (solid: equation 17). The instantaneous mass of the protostar is used as a time coordinate. Also shown is that without dark-matter gravity (dashed).

$t_{\text{KH}} = GM_*^2 / R_* L_*$: since it takes a Kelvin-Helmholtz timescale for a protostellar cloud to contract enough to ignite nuclear fusion, the mass where these two timescales become equal corresponds to the mass of an accreting protostar when it reaches the main sequence. Note that in deriving the mass-scale of the stars by equating these two timescales, O’Shea et al. (2005) implicitly assumed that the accretion is halted by an unknown mechanism at the onset of the hydrogen burning. For comparison with O’Shea et al. (2005), if we adopt the same timescale argument, the stellar mass becomes $\sim 16 M_{\odot}$ in our case, with the timescales $\sim 2.2 \times 10^5$ yr. In this evaluation, we used the stellar parameters listed in Schaerer (2002). This stellar mass-scale is similar to that by O’Shea et al. (2005) owing to the similar accretion rate to theirs ($\sim 10^{-4} M_{\odot} \text{yr}^{-1}$). This lower accretion rate compared with that of the first stars ($10^{-2} - 10^{-3} M_{\odot} \text{yr}^{-1}$) is due to lower temperature by the HD cooling in our case, while in O’Shea et al. (2005) it is due to high angular momentum of the star forming clumps. If we included both of these effects, the accretion rate and then the stellar mass-scale would be even lower.

Johnson & Bromm (2005) and Shchekinov & Vasiliev (2005) stressed the importance of HD chemistry in the early universe, studying evolution of gas ionized by strong shocks. This situation is similar to that supposed by Uehara & Inutsuka (2000). Although the cause of ionization is different from ours, the final consequence is similar: the HD formation is facilitated by ionization and the temperature declines as low as the CMB temperature. Johnson & Bromm (2005) also mentioned the evolution of fossil HII regions and pointed out the importance of HD. They suggested that the second-generation stars have lower mass than the first-stars owing to the lower temperature environment. We here confirmed their claim by more detailed calculations.

In this paper, we do not include external radiative heating, except for the CMB radiation in our calculation. By comparing runs with and without CMB radiation, we find that the sole effect of the CMB radiation is preventing the gas from falling below the radiation temperature: it does not alter the higher temperature behavior at all. If the first stars have already created the UV background

radiation, we need to take account of such effects as photoionization/dissociation and photo-heating. Oh & Haiman (2003) discussed that in the presence of a UV radiation field, subsequent star formation is prevented in fossil HII regions. As a future work, we are planning to include effects of the UV field in our calculation and examine the validity of their claim.

Finally, we need to consider the effect of a remnant BH. The radiation from the gas accreted onto a BH can affect the surrounding gas. However, O’Shea et al. (2005) indicated that photodissociation flux expected from this is insufficient to alter the H₂ fraction significantly. The BH also has an effect on the gas dynamics through the gravitational field. The length scale of the region influenced by the BH gravity is given by the Bondi accretion radius

$$r_{\text{Bondi}} \sim 3.3 \times 10^{-3} \left(\frac{T}{10^4 \text{K}} \right)^{-1} \left(\frac{M_{\text{BH}}}{100 M_{\odot}} \right) \left(\frac{\mu}{0.6} \right) \text{ pc}, \quad (18)$$

where M_{BH} and μ are the BH mass and the mean molecular weight of the gas, respectively. The mass inside the Bondi radius is initially negligible compared to the total mass of the collapsing gas. With cooling and contraction, however, the Bondi radius becomes as large as the central core radius. Therefore if the BH exists exactly at the center of the halo, all the cooled gas is eventually accreted into the BH, instead of forming the next generation of stars. However, even in the case of direct BH formation, part of the mass is likely to be shed non-spherically. If so, the BH would be kicked out of the shallow potential wells of small halos, or even if it could remain inside the halo, it would be off-center. In these cases, the second-generation star formation occurs as shown in our calculation.

5 SUMMARY

We have investigated the evolution of photo-ionized gas in small halos since the death of the exciting first star, by using one-dimensional hydrodynamics incorporating primordial gas chemistry. We have found that the high electron fraction induces molecular hydrogen formation in a larger amount than in a cloud without initial ionization. The enhanced H₂ cooling makes temperature in the central region lower than the threshold value for HD formation. The cooling by HD further drops the temperature below 100 K. We have also shown that the gas in halos with $\gtrsim 10^6 M_{\odot}$ cools sufficiently and subsequently forms stars. In those HD-cooling halos, the gas collapses further at < 100 K and eventually fragments into low-mass cores. Inside these cores, low-mass stars are expected to form. The nature of second-generation stars can be quite different from that of first stars despite being composed of the same material.

ACKNOWLEDGMENTS

The authors would like to thank Tom Abel for fruitful discussion, Toshitaka Kajino for continuous encouragement, and the referee, Emanuele Ripamonti, for valuable comments improving the manuscript. This work is supported in part by the Grants-in-Aid by the Ministry of Education, Science and Culture of Japan (16204012:KO).

REFERENCES

- Abel T., Anninos P., Zhang Y., Norman M. L. , 1997, *NewA*, 2, 181
 Abel T., Bryan G. L., Norman M. L. , 2002, *Science*, 295, 93
 Bromm V., Coppi P. S., Larson R. B. , 2002, *ApJ*, 564, 23
 Bromm V., Ferrara A., Coppi P. S., Larson R. B., 2001, *MNRAS*, 328, 969
 Bromm V., Yoshida N., Hernquist L. , 2003, *ApJ*, 596, L135
 Ciardi B., Ferrara A., *Space Science Reviews*, 116, 625
 Christlieb N., et al., 2002, *Nature* 419, 904
 Dalgarno A., McCray R. A., 1972, *ARA&A*, 10, 375
 Frebel A., et al., 2005, *Nature* 434, 871
 Galli D., Palla F. , 1998, *A&A*, 335, 403
 Galli D., Palla F. , 2002, *PSS*, 50, 1197
 Glover S. C. O., Brand P. W. J. L. , 2001, *MNRAS*, 321, 385
 Heger A., Woosley S. E. , 2002, *ApJ*, 567, 532
 Johnson J. L., Bromm V., pre-print(astro-ph/0505304)
 Kitayama T., Yoshida N., Susa H., Umemura M., 2004, *ApJ*, 613, 631
 Kogut A. et al., 2003, *ApJS*, 148, 161
 Larson R. B., 1969, *MNRAS*, 145, 271
 MacLow M. M., Shull J. M., 1986, *ApJ*, 302, 585
 Mihalas D., Mihalas B.W., 1984, *Foundations of Radiation Hydrodynamics* (New York:Oxford Univ. Press)
 Nakamura F., Umemura M. , 2002, *ApJ*, 569, 549
 Navarro J. F., Frenk C. S., White S. D. M. , 1997, *ApJ*, 490, 493
 Oh S. P., Haiman Z. , 2003, *MNRAS*, 346, 456
 Omukai K., Nishi R. , 1998, *ApJ*, 508, 141
 Omukai K., Nishi R. , 1999, *ApJ*, 518, 64
 Omukai K., Palla F. , 2003, *ApJ*, 589, 677
 Omukai K., Tsuribe T., Schneider R., Ferrara A., 2005, *ApJ*, 626, 627
 O’Shea B. W., Abel T., Whalen D., Norman M. L., 2005, *ApJ*, 628, L5
 Penston M. V., 1969, *MNRAS*, 144, 425
 Romano D., Tosi M., Matteucci F., Chiappini C., 2003, *MNRAS*, 346, 295
 Rybicki G. B., Lightman A. P., 1979, *Radiative Processes in Astrophysics*, New York:Wiley
 Schaerer D., 2002, *A&A*, 382, 28
 Schneider R., Ferrara A., Natarajan P., & Omukai K., 2002, *ApJ*, 571, 30
 Shapiro P. R., Kang H., 1987, *ApJ*, 318, 32
 Shchekinov Y. A., Vasiliev E. O., pre-print(astro-ph/0505619)
 Shu F. H., 1977, *ApJ*, 214, 488
 Spergel D. N., et al., 2003, *ApJS*, 148, 175
 Thoul A. A., Weinberg D.H., 1995, *ApJ*, 442, 480
 Uehara H., Inutsuka S., 2000, *ApJ*, 531, L91
 Umeda H., Nomoto K., 2002, *ApJ*, 565, 385
 Wada K., Venkatesan A., 2003, *ApJ*, 591, 38
 Whalen D., Abel T., Norman M. L. , 2004, *ApJ*, 610, 14
 Yamada M., Nishi R., 1998, *ApJ*, 505, 148
 Yoshii Y., 1981, *A&A*, 97, 280